

# Harmonic Analysis in a Power System with Wind Generation

Stavros A. Papathanassiou, *Member, IEEE*, and Michael P. Papadopoulos, *Member, IEEE*

**Abstract**—Variable-speed wind turbines inject harmonic currents in the network, which may potentially create voltage distortion problems. In this paper, a case study is presented for a 10-MW wind farm, intended to be connected to a network with extended high-voltage submarine cable lines. First, the system modeling approach and the harmonic load-flow calculation is described. Then, the harmonic impedance of the system is calculated for a variety of configurations and operating conditions, and its main characteristics are discussed. Harmonic load-flow calculations are provided to indicate potential voltage distortion problems. A simplified methodology, suggested in relevant IEC publications, is applied to the system and its results are compared to those of the harmonic load flow. A discussion on the summation of harmonic currents within a wind farm is also included.

**Index Terms**—Harmonics modeling, power system harmonics, summation of harmonics, wind turbines.

## I. INTRODUCTION

ALTHOUGH variable-speed wind turbines (WTs) are grid-friendly machines in most power quality respects, harmonics generated by the grid-side power converters may be of concern in networks, where harmonic resonance conditions may exist [1]. Performing a detailed and accurate harmonic analysis in a real-life power system is a quite complicated issue, involving advanced models for all system components, including the consumer loads, which present the greatest uncertainties [2]–[8]. In the case of distributed wind generation resources connected to the distribution network, performing sophisticated harmonic load-flow studies is not a usual practice due to the large number of such installations and their relatively small size and significance [typically a few megawatts per installation, for connection to the medium-voltage (MV) network]. Hence, simplified assessment methods are usually adopted to provide fast results, based on conservative (safe-side) assumptions [9].

In this paper, the harmonic analysis is performed for a study case system, which involves a  $20 \times 500\text{-kW}$  wind farm, consisting of variable-speed WTs, to be connected to the medium voltage (MV) network of the Greek island of Kefalonia. The islands Kefalonia, Lefkas, and Zakynthos, located in the Ionian Sea in western Greece, are connected to the mainland HV grid by successive overhead and submarine line sections of significant length as shown in Fig. 3 (Section III). The large capacitance of the submarine cables, which might give rise to harmonic resonance conditions, warranted an investigation to rule

Manuscript received February 3, 2005; revised June 27, 2005. Paper no. TPWRD-00066-2005.

The authors are with the School of Electrical and Computer Engineering, National Technical University of Athens (NTUA), Athens 15780, Greece (e-mail: st@power.ece.ntua.gr).

Digital Object Identifier 10.1109/TPWRD.2005.864063

out possible voltage harmonic distortion problems due to the WT output current harmonics.

The adopted modeling methodology is outlined in Section II. The studied system is described in Section III. Results from the harmonic simulation are provided in Section IV, to show the effect of various parameters on the harmonic impedance of the system and to indicate potential voltage distortion issues. In Appendix A, a simplified evaluation methodology from IEC 61 000-3-6 [10] is applied and its results are compared to those obtained from the harmonic simulation. The important issue of the summation of harmonic currents due to individual WTs is discussed in Appendix B.

## II. MODELING OF THE SYSTEM

### A. Fundamental Principles

The modeling approach adopted in this paper permits the basic representation of the system harmonic impedance variation at all buses and the execution of harmonic load-flow calculations to determine the resulting voltage distortion.

Models and applied methodologies are based on relevant CIGRE guides [2]–[4], the IEEE Task Force recommendations [5], [6] as well as on the relevant literature (e.g., [7] and [8]). Specific models of system components are presented in Section III (including components such as rotating electric machines, not present in the case study system). It is stressed that more sophisticated models exist for each component. However, their application is usually contradicted by the lack of reliable data, as well as by the oversimplified representation of other components (particularly the consumer load). The following shows the fundamental assumptions and considerations adopted in this paper.

- Harmonic sources are modeled as current injections of given amplitudes per frequency. This assumption is justified for current-controlled converters with PWM hysteresis controllers, as is the case with the output converters of the examined WTs.
- A direct harmonic solution is obtained [7], that is, the coupling between harmonics of different order is ignored.
- The network is modeled by its three-phase equivalent, transformed in the symmetrical component domain. Thus, the propagation of zero-sequence harmonics is properly represented and possible differences in the positive- and negative-sequence characteristics of the system are accounted for.

### B. Harmonic Load Flow

The harmonic load flow at frequency  $f_h = h \cdot f_1$  (where  $h$  is not necessarily an integer) is based on the solution of the set of linear equations

$$[I_h] = [Y_h][V_h] \quad (1)$$

where  $[I_h]$  is the vector of the nodal harmonic current injections of each bus,  $[V_h]$  is the vector of the resulting harmonic voltages, and  $[Y_h]$  is the network admittance matrix at frequency  $f_h$ .

The formulation of the admittance matrix of the network is a standard power system analysis practice, using characteristic equations for all network elements (lines, transformers, rotating machines, etc.), as discussed in the following. Here, the sequence (positive, negative, zero) equivalents of the network components are used. Equation (1) can be solved simultaneously for the three sequences, as a set of  $3N \times 3N$  equations, where  $N$  is the number of system buses. Then, each element of vectors  $[I_h]$  and  $[V_h]$  is a  $3 \times 1$  subvector, comprising the three sequence components of the harmonic current or voltage of a specific bus. Similarly, each element of matrix  $[Y_h]$  is a  $3 \times 3$  submatrix, the nondiagonal elements of which are zero for symmetrical network elements.

Inverting  $[Y_h]$  yields the network harmonic impedance matrix  $[Z_h]$ . Its diagonal elements  $Z_{h,ii}$  are the harmonic self-impedances of the respective buses. The nondiagonal elements  $Z_{h,ij}$  are transfer impedances, related to the effect on the voltage of bus  $i$  when a harmonic current is injected at bus  $j$ . Calculating  $[Z_h]$  for varying frequencies  $f_h = h f_1$  is known as a “frequency scan,” which reveals possible harmonic resonance conditions of self or transfer impedances.

### C. Harmonic Sources

Since harmonic sources are treated as current injections, to completely describe a three-phase source, three current phasors (magnitudes and angles) per harmonic frequency would be required. Data available in practice, however, usually comprise only one current magnitude per frequency (for instance, as in the power quality certificates per IEC 61 400-21, [11]). Based on such data, the modeling should account for superposition (summation) effects of harmonics from different sources, as well as for the sequence characteristics of harmonic current injections.

For the summation of harmonics, the second summation law of [10] is adopted, as it is recommended in the WT power-quality assessment standard IEC 61 400-21 [11]

$$I_h = \sqrt{\sum_k I_{h,k}^2} \quad (2)$$

where  $I_{h,k}$  is the  $h$ th order contribution from source  $k$ . Values recommended in [10] and [11] for the summation exponent are  $\alpha = 1.0$  for  $h < 5$ ,  $\alpha = 1.4$  for  $5 \leq h \leq 10$ , and  $\alpha = 2.0$  for  $h > 10$ , reflecting the fact that individual harmonic vectors tend to become uncorrelated at higher frequencies. For harmonic sources connected at different buses, their phase angles and possibly their magnitudes may be considered to be random variables, with increasing variance as the harmonic order  $h$  increases, to create a summation effect similar to (2). Further discussion on the summation of harmonics is included in Appendix B.

Typical power system harmonics (e.g., associated with iron saturation or line-commutated converters) present known sequence characteristics (positive, negative, and zero sequence, for  $h = 3k + 1$ ,  $3k - 1$ , and  $3k$ , respectively). These are easily

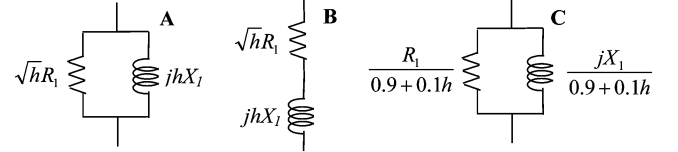


Fig. 1. Alternative harmonic models considered for the system load.

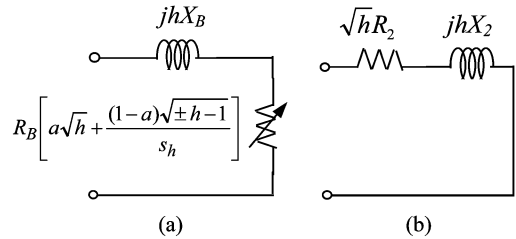


Fig. 2. (a) Induction and (b) synchronous machine harmonic equivalents.

reproduced by properly setting the angles of phases  $b$  and  $c$  with respect to phase  $a$ :  $\varphi_{b,h} = \varphi_{a,h} - h \cdot (2\pi/3)$ ,  $\varphi_{c,h} = \varphi_{a,h} + h \cdot (2\pi/3)$ . The harmonics of the switching converters, however, may completely deviate from the standard sequence characteristics, as is the case with hysteretic pulsewidth-modulated (PWM) controllers. In this case, all high-order harmonics may include positive- and negative-sequence components, but not zero-sequence ones when the source does not permit it (delta-connected windings, three-leg converters, etc.).

### D. System Load

The proper selection of the load model is very important for correctly assessing the magnitude of harmonic resonances. However, no generally applicable harmonic model exists and case-specific measurements and evaluations are needed for detailed studies.

From the variety of harmonic load models proposed in the literature, three alternative representations are shown in Fig. 1, selected for their simplicity [2]–[5]. In all cases,  $R_1$  and  $X_1$  are the fundamental frequency resistance and reactance, corresponding to the nominal power of the load. Results from the application of these models are included in Section IV.

### E. Electric Machines and Transformers

Asynchronous machines are simulated using their simplified equivalent circuit, referred to the harmonic frequency  $f_h = h \cdot f_1$ , shown in Fig. 2(a).  $R_B$  and  $X_B$  are the resistance and reactance, as determined from the blocked-rotor test. The factor  $\alpha = R_1/R_B$ , where  $R_1$  is the resistance of the stator, has typical values of 0.45–0.50. The slip at frequency  $f_h = h \cdot f_1$  is given by

$$s_h = \frac{\pm h\omega_1 - \omega_r}{\pm h\omega_1} \quad (3)$$

where  $\omega_r$  is the rotor speed and the + or – sign depends on the sequence (positive or negative) of the considered harmonics. More accurate results may be obtained using the steady-state equivalent for double cage rotor [7]. More detailed models are

TABLE I  
PARAMETER VALUES FOR THE TRANSFORMER MODEL OF (5) (FROM [4])

	$c_0$	$c_1$	$c_2$	$b$
Small T/F	0.85-0.90	0.05-0.08	0.05-0.08	0.9-1.4
Large T/F	0.75-0.80	0.10-0.13	0.10-0.13	0.9-1.4
<i>under the constraint <math>c_0+c_1+c_2=1</math></i>				

also available (e.g., [13]), which are suited for the analysis of specific motors.

Synchronous machines are simulated as shown in Fig. 2(b), where  $R_2$  and  $X_2$  are the negative-sequence resistance and reactance, often approximated using the  $d$  and  $q$  axis subtransient reactances

$$X_2 = \frac{(X_d'' + X_q'')}{2}. \quad (4)$$

For the zero sequence, the neutral grounding impedance of a Y-connected stator winding is taken into account.

In the positive and negative sequence, transformers are modeled by their series harmonic impedance  $Z_{k,h} = R_{k,h} + jhX_k$ , where

$$R_{k,h} = R_k(c_0 + c_1h^b + c_2h^2). \quad (5)$$

$R_k$  and  $X_k$  are the short-circuit resistance and reactance at the fundamental frequency. Values for the parameters of (5), given in [4], are summarized in Table I.

#### F. Transmission Lines and Shunt Elements

Overhead lines and cables are modeled using multiple nominal  $\pi$  sections, connected in series. According to [7], an error of less than 1.2% is achieved using three nominal  $\pi$  sections for each line segment whose length is equal to 1/4 of the wavelength (1500 km at 50 Hz). Since the analysis extends to the 50th harmonic order (1/4 wavelength = 30 km at 2.5 kHz), satisfactory results are obtained using one  $\pi$  section for every 10 km of a 150-kV overhead line. Better accuracy has been sought for the submarine cables, responsible for the HV system shunt capacitance, using one  $\pi$  section per 1.5 km of 150-kV cable line. The line modeling accuracy can be further improved by using the equivalent  $\pi$  model [7], [8], [12].

Shunt elements considered are basically compensating reactor coils and capacitors, which are modeled as concentrated impedances.

### III. STUDY CASE SYSTEM

The one-line diagram of the power system under study is shown in Fig. 3. Reactor coils are installed at the substations of all islands, to compensate the high capacitance of the oil-insulated HV submarine cables (350 nF/km) at minimum load. Each HV/MV substation includes two transformers: Dyn11, 20/25 MVA (ONAN/ONAF), operating in parallel (MV bus-section breaker closed). The secondary neutral is grounded via a 10- $\Omega$  earth-fault current-limiting resistor.

The MV network of the Argostoli substation, where the wind farm is to be connected, comprises several hundred kilome-

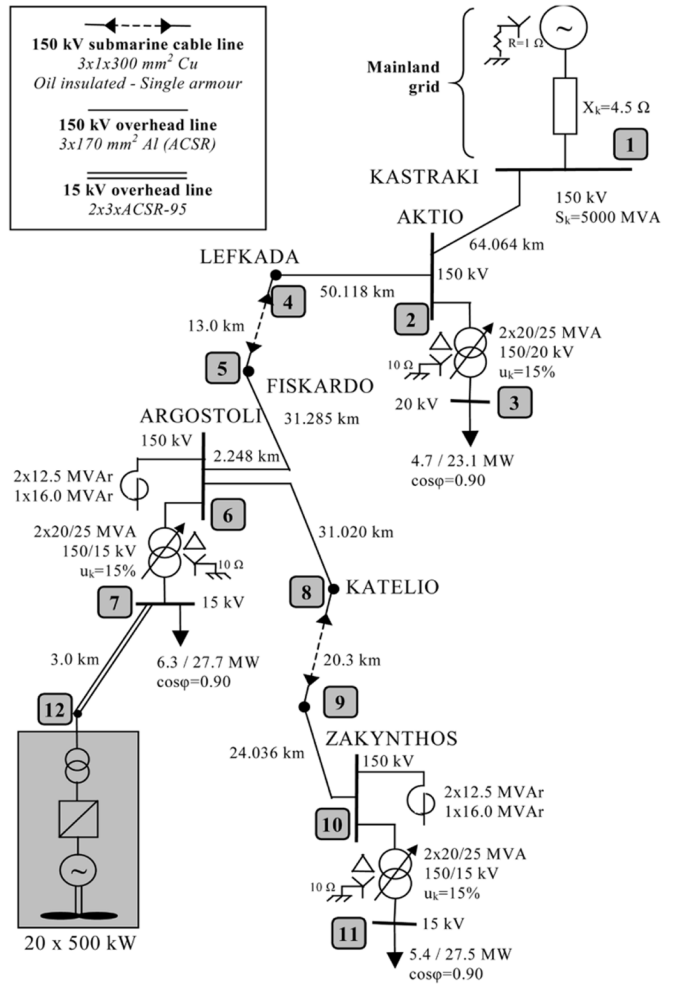


Fig. 3. One-line diagram of the study case system.

ters of overhead 15-kV lines (shunt capacitance  $\sim 5$  nF/km), as well as a 15-kV submarine cable line ( $4 \times 1 \times 95$  Cu, 6.5 km, 300 nF/km). The total shunt capacitance of this network is approximately evaluated at  $\sim 6 \mu\text{F}$  (400 kVAr). In a simplified representation, to account for the first order resonance at the point of common coupling (PCC) of the wind farm (Argostoli MV bus), this aggregate capacitance is considered directly connected to the MV busbars, in a Y-grounded configuration.

The wind farm consists of  $20 \times 500$ -kW variable speed WTs and it is intended to be connected to the MV busbars of the Argostoli substation, via a dedicated, double-circuit overhead line (Fig. 3). The measured output current waveform and harmonic spectrum of the examined wind turbines are shown in Fig. 4. Since the measurements have been performed at the MV side of the Dyn11 WT transformer, the currents can only include positive- or negative-sequence components [14]. The harmonic spectrum is mainly located between 1.0 and 1.5 kHz, a range associated with the switching of the hysteresis PWM current controllers of the grid-side converter. Notably, the measurements shown in Fig. 4 concern a relatively old machine. Modern turbines of the same type present significantly improved harmonic spectra.

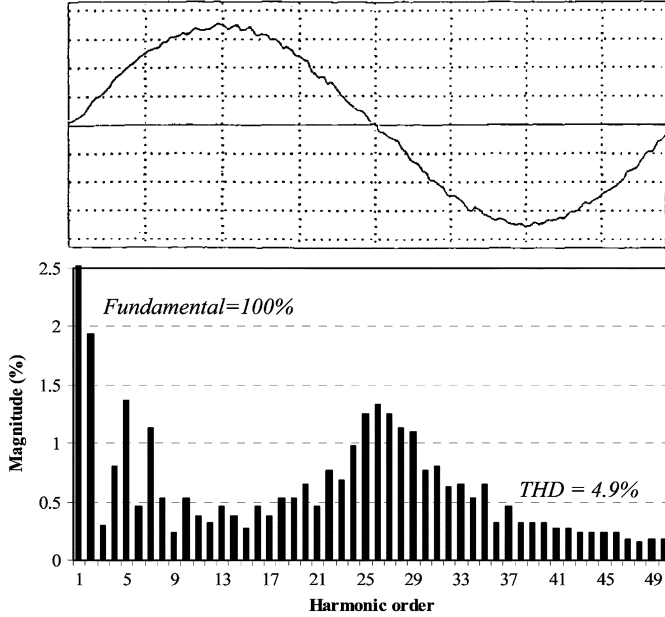


Fig. 4. Measured current waveform and harmonic spectrum of the WT output current.

#### IV. APPLICATION RESULTS

##### A. Harmonic Impedance Characteristics

The voltage harmonic distortion  $U_{h,i}$  at node  $i$ , created by the injection of harmonic current  $I_{h,i}$  at node  $j$  of the system is given by

$$U_{h,i} = Z_{h,ij} \cdot I_{h,j} \quad (6)$$

where  $Z_{h,ij}$  is the element  $ij$  of the harmonic impedance matrix  $[Z_h]$  (self-impedance if  $i = j$ , transfer impedance otherwise). Given the harmonic current injection, applying (6) to find  $U_h$  becomes then an issue of evaluating  $Z_h$ . Voltage distortion problems at a certain frequency (order  $h$ ) will arise when either  $I_h$  is excessive or  $Z_h$  is high, typically because of parallel LC resonance effects in the system.

The fundamental harmonic characteristics of the studied system can be observed in the diagrams of Figs. 5 and 6, showing the variation of the system impedance with the harmonic frequency, at the 15- and 150-kV busbars of Argostoli. The frequency scan has been performed for minimum and maximum system load. At the MV busbars, the variation of the harmonic impedance is dominated by the first parallel resonance of the aggregate busbar capacitance (400 kVAr) with the upstream system inductive impedance (short-circuit capacity  $S_k \approx 150$  MVA), further discussed in Appendix A. Up to the resonance frequency, at  $\sim 1.2$  kHz, the system is basically inductive, becoming capacitive thereafter. At the HV side (Fig. 6), the diagram exhibits several resonance peaks, associated with the multiple cable/line sections. The lowest frequency peak at approximately 100 Hz (also discernible in Fig. 5), is associated with the first-order resonance of the total HV shunt capacitance with the upstream system series inductance. At the frequencies of interest, the system impedance is inductive up to 2.0–2.5 kHz.

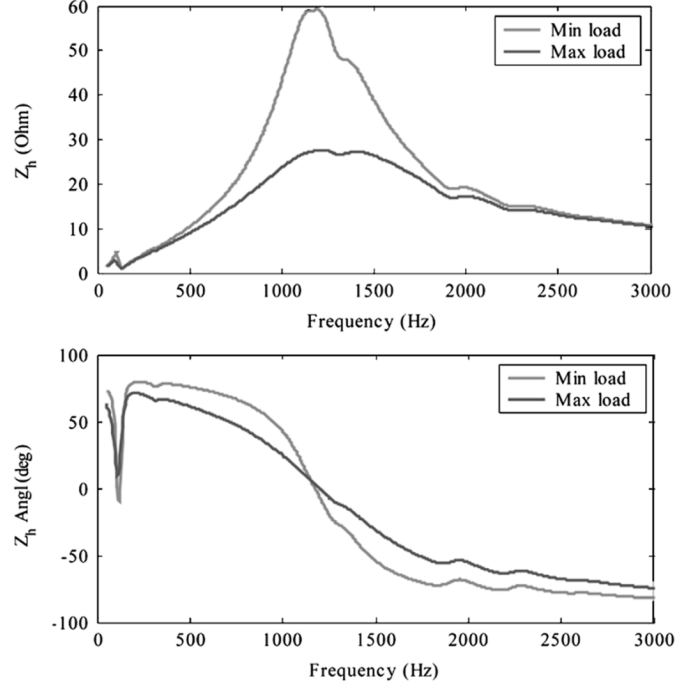


Fig. 5. Magnitude and angle of the harmonic impedance at the PCC of the wind farm (Argostoli 15-kV busbars), for maximum and minimum load conditions.

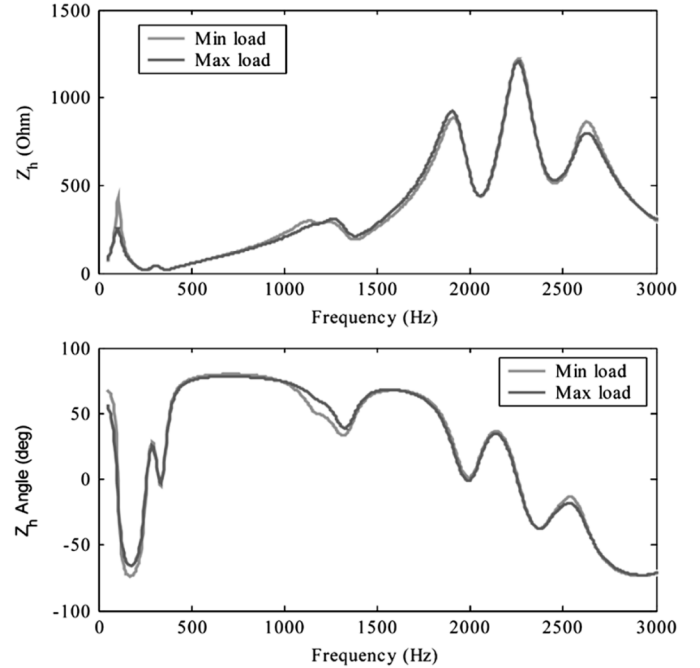


Fig. 6. Magnitude and angle of the harmonic impedance at the 150-kV busbars of Argostoli, for maximum and minimum load conditions.

The harmonic impedance of the system at a specific bus will depend on its operating configuration and the load level. The effect of the load, illustrated in Figs. 5 and 6, is clear at the MV side of the substation. At minimum load conditions, the impedance magnitude increases by a factor of 2.0, as lightly loaded systems are known to exhibit more pronounced resonance peaks. The impedance at the HV side of the substation is much less affected by variations of the load.

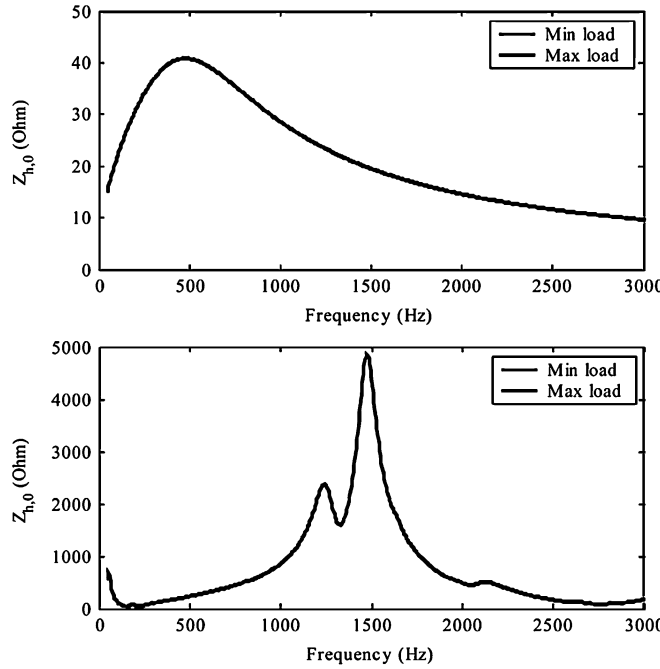


Fig. 7. Magnitude of the zero-sequence harmonic impedance at the MV and HV busbars of Argostoli, for maximum and minimum load conditions.

The magnitude of the zero-sequence harmonic impedance for the same buses is shown in Fig. 7. Since no zero-sequence harmonic excitation exists, due to the D-connected MV windings of the WT transformers,  $Z_{h,0}$  is shown solely for information purposes. A main differentiating factor, compared with the positive and negative sequence, is the effective isolation of adjacent voltage levels (HV-MV-LV) by the Dy-connected HV/MV and MV/LV transformers. Hence, the load variations have no effect at all on  $Z_{h,0}$ .

The effect of the harmonic model used to represent loads is illustrated in Fig. 8. Results are shown for the MV and HV buses at Argostoli, obtained using the three different models of Fig. 1. First of all, it is observed that the load modeling is critical for the local MV bus impedance, but not so much for the HV system. Model C yields results with too much damping at high frequencies, since its resistive and inductive branches are effectively shorted for large values of  $h$  (Fig. 1). This model is better suited for low-order harmonics. Comparing Models A and B, the latter tends to reduce the damping effect of the load due to the series RL connection. Model A is selected for application here, its shunt inductance corresponding to the aggregate load of small induction motors within the MV and LV network, which do not provide essential damping at high frequencies. All results presented in the paper are based on this model.

Operation of the system at different load levels involves switching in and out of the compensating shunt reactors. To maintain an acceptable voltage profile over the network, all coils are connected at minimum load conditions. At the maximum load, only one 12.5-MVAr reactor is connected at Argostoli. The effect of the compensating coils has been studied and it was not found to be of primary importance. They affect the resonance peak of the MV impedance (15% change between the extreme compensation cases for the same load conditions),

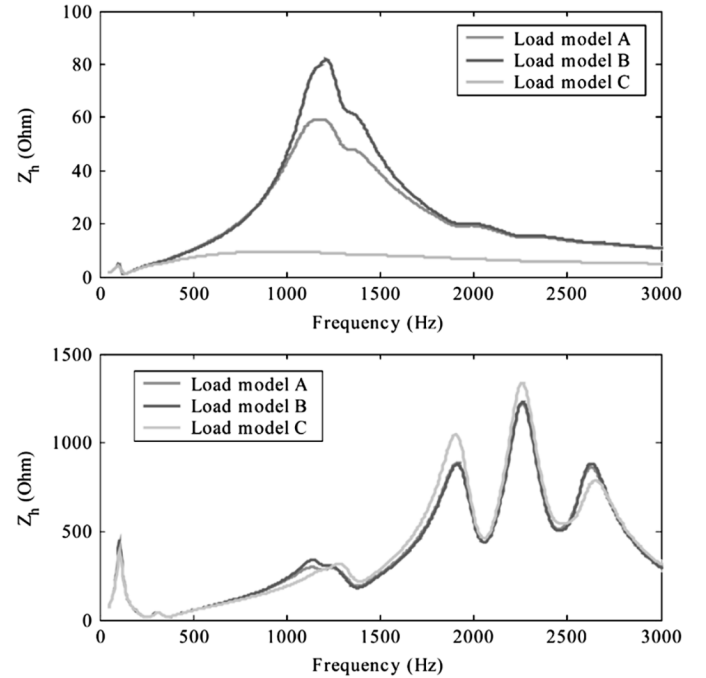


Fig. 8. Magnitude of the harmonic impedance at the MV and HV busbars of Argostoli, for the three load models of Fig. 1.

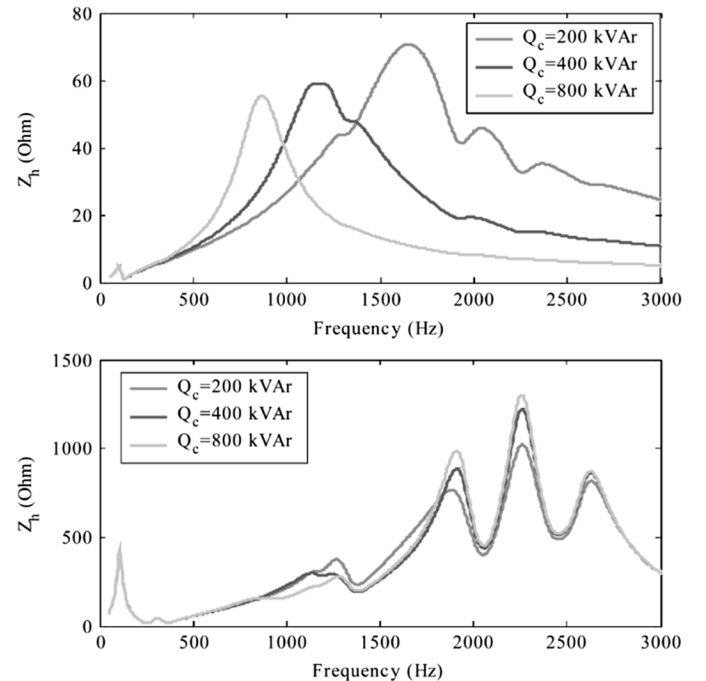


Fig. 9. Magnitude of the harmonic impedance at the MV and HV busbars of the Argostoli substation, for different MV aggregate capacitance.

whereas they also influence the first resonance frequency of the HV impedance at around 100 Hz.

Since the current spectrum of the considered harmonic sources is concentrated around the 25th order, variations of the PCC harmonic impedance in the frequency range 1.0–1.5 kHz are most critical. The resonance frequency in this range varies inversely with the aggregate capacitance  $Q_c$  connected to the MV busbars, as shown in Fig. 9.  $Q_c$  represents the total shunt

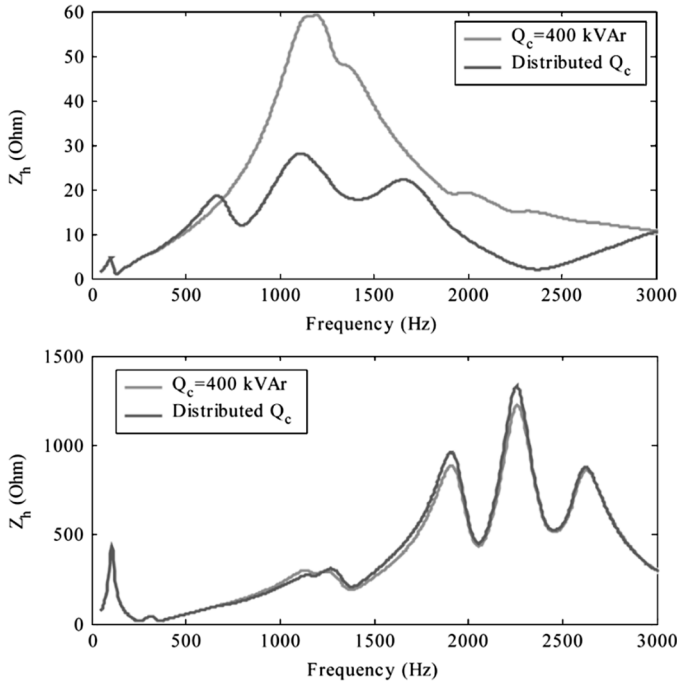


Fig. 10. Effect of network capacitance representation on the magnitude of the harmonic impedance at the MV and HV busbars of Argostoli.

capacitance of the whole MV network and its value is not exactly known. The adopted  $Q_c = 400$  kVAr, besides being a reasonable estimation, based on available network data, represents also a worst-case scenario, producing a resonance within the high spectral content area of the current (Fig. 4).

In the previous analysis, the local MV network of the Argostoli substation was drastically simplified to an aggregate load and capacitance. This network consists of eight feeders, with an average length of 70 km/feeder, including the laterals, serving in total several hundreds of MV/LV distribution substations. Although its detailed modeling is practically not feasible, a more accurate representation has been implemented, after the reduction of the number of nodes per feeder. Further, the shunt capacitance of the internal MV cable network of the wind farm can also be considered ( $\sim 12$  km of cable lines, with 250-nF/km shunt capacitance, resulting in a total capacitance of  $3 \mu\text{F}$  per phase, connected at bus 12). The total capacitance of the MV network in this detailed representation is  $7.75 \mu\text{F}$  ( $Q_c = 550$  kVAr), distributed over the network, instead of being concentrated at the MV busbars.

The system harmonic impedance, applying the enhanced MV network representation, is illustrated in Fig. 10 for minimum load conditions. A more complex harmonic behavior is now observed, with several higher order resonance peaks, which cannot be isolated and attributed to specific elements. A wide region of increased harmonic impedance values around 1.0–1.5 kHz is still present, but the impedance peak is greatly reduced, indicating that the simplified aggregate capacitance approach is more conservative. Regarding the HV side, the representation of the MV network is clearly of secondary importance and it would not have been justified if only the HV system harmonics were of interest.

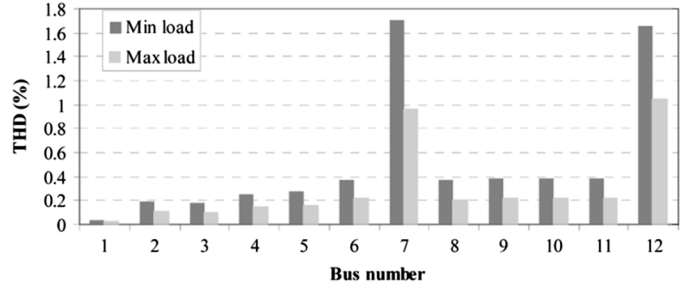


Fig. 11. THD coefficient at all system buses, at minimum and maximum load conditions, calculated with the simplified MV network model.

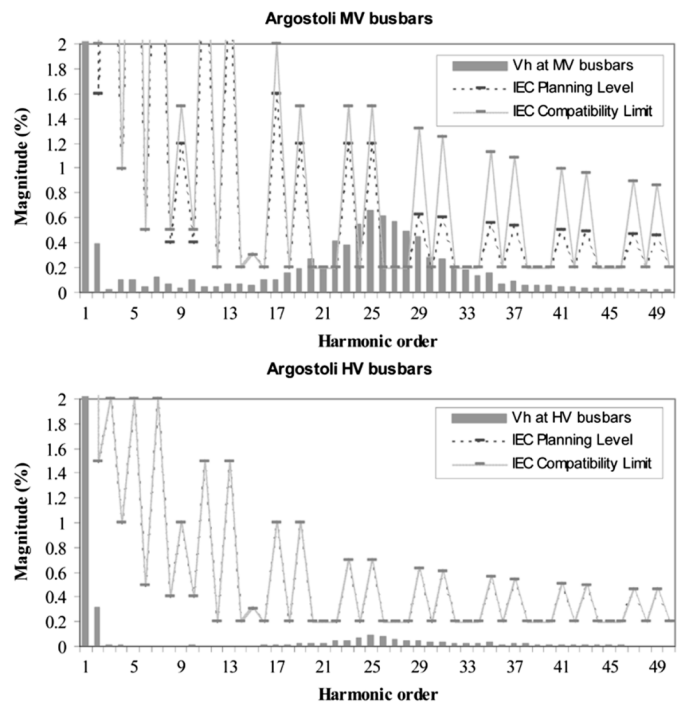


Fig. 12. Voltage distortion per harmonic order at the MV and HV busbars of Argostoli, for minimum load conditions, calculated with the simplified MV network model.

### B. Harmonic Load-Flow Results

After presenting the characteristics of the system harmonic impedance and its dependence on various parameters, results are now presented regarding the resulting voltage distortion.

The calculated voltage THD coefficients for the 12 buses of the system are shown in Fig. 11, for minimum and maximum load conditions, using the simplified but conservative aggregate impedance model for the MV network. The harmonic distortion of the voltage is increased at minimum load, as expected from the analysis of the previous section, as well as nearest the wind farm (buses 12 and 7). Nevertheless, the calculated THD values are too small to be of any concern.

A reason for concern appears when the voltage distortion at individual harmonic orders is examined and compared to limit values. This is shown in Fig. 12 for the MV and HV buses of Argostoli substation, at minimum load conditions. A relatively high voltage distortion appears at the MV busbars between 1.0 kHz–1.5 kHz, associated with the resonant peak of the system

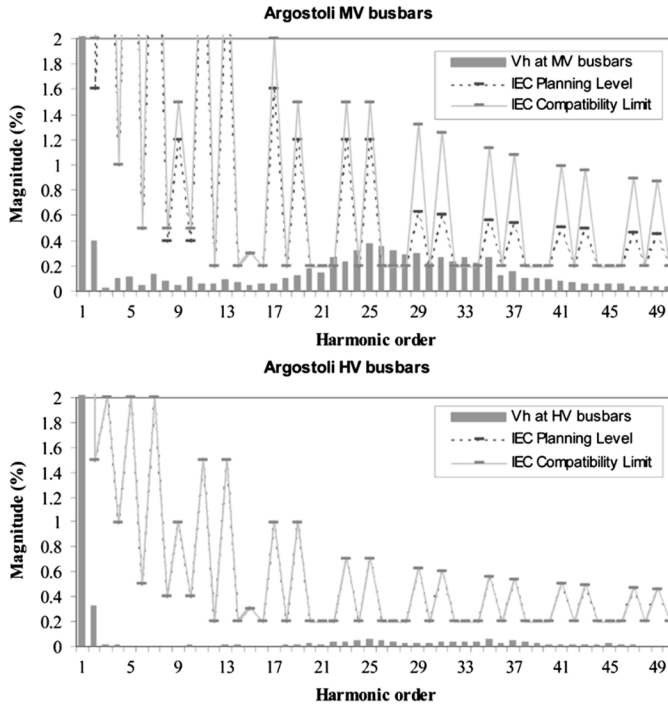


Fig. 13. Voltage distortion per harmonic order at the MV and HV busbars of Argostoli, for minimum load conditions, using the detailed MV network representation.

impedance (Fig. 5), which coincides with the harmonic excitation spectrum (Fig. 4). At the HV side, the voltage distortion is very reduced.

On the diagrams of Fig. 12, the compatibility limits and the indicative planning levels of IEC 61 000-3-6 are also marked for comparison purposes. If these planning levels were accepted by the utility as permissible distortion values for the specific wind farm, violations would occur for harmonics of even and triplen orders, between 1.0 and 1.5 kHz. The situation would have been further aggravated if the utility applied a limit allocation procedure [9], [10], in which case, an individual user of the network is allocated only a portion of the total available voltage distortion limit. At the frequency range around the ripple control frequency (175 Hz in Greece), the calculated voltage distortion is acceptably low.

If the detailed MV network representation is applied, the calculated voltage distortion is shown in Fig. 13. Harmonics are now reduced in the critical frequency region, although still exceeding the IEC planning levels at certain frequencies.

The results presented in this section demonstrate the need for a detailed representation of the system, particularly at the local MV level, if a reliable evaluation of the resulting harmonic distortion is sought. Yet, the basic modeling already provides a clear indication of potential problems, while the application of too elaborate models may be rendered superfluous by the great uncertainties in the load representation. Notably, the need for a detailed modeling approach exists only when the focus is in the local MV network. For the HV system, the crude aggregation of the MV load and capacitance is clearly sufficient.

At this point, it should be mentioned that in real-world situations, the average utility would not perform a harmonic analysis

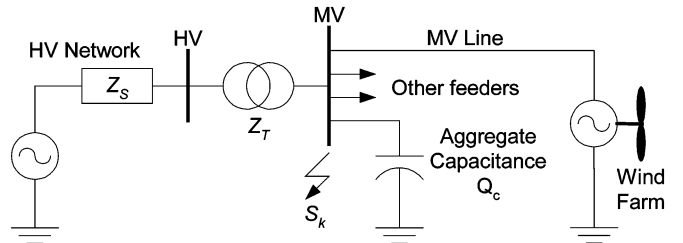


Fig. 14. Simplified representation of the system for hand calculation of the first harmonic resonance.

of any greater detail for a single 10-MW wind farm. Rather, simplified analysis methods are usually employed, as the one presented in Appendix A, which provides fast and safe (albeit, too conservative in many cases) estimations.

A further issue with modern WTs and other distributed generation (DG) types is the high-frequency content of their output current, which often extends well beyond the 2–3-kHz range. At such frequencies, the harmonic models used for the network components (and particularly the loads) are not suitable, while no specific distortion limits are stipulated in the regulations (utilities often adopt a uniform 0.2% voltage distortion limit [9]).

## V. CONCLUSION

In this paper, a harmonic penetration study has been presented for a power system where a wind farm, consisting of variable-speed turbines, is scheduled to be connected. After presenting the system modeling approach, application results are given from the frequency scan and the harmonic load-flow analysis. The harmonic characteristics of the system and their sensitivity with respect to operating and modeling parameters have been discussed. Potential voltage distortion problems have been identified due to the coincidence of the first harmonic resonance frequency of the system with the peak of the harmonic spectrum of the WT current. Nevertheless, harmonic distortion issues appear only for the local MV network and not for the HV system, which was the initial point of concern.

## APPENDIX A

In the following, the simplified and easily applicable harmonic distortion evaluation method of IEC 61 000-3-6, [9], [10] is applied to the study case system and its results are compared with those obtained by the harmonic load flow.

Applying the guidelines of [10], a first evaluation of the frequency  $f_r$  of the first order resonance at the MV level can be obtained by using the heavily simplified equivalent shown in Fig. 14. The total network capacitance is concentrated at the MV busbars, whereas the upstream system is represented by its Thevenin impedance, related to its short-circuit capacity  $S_k$ . All other installations are ignored. In this system, the resonance frequency  $f_r$  is given by

$$f_r = f_1 \sqrt{\frac{S_k}{Q_c}} \quad (7)$$

The short circuit capacity at the MV and HV busbars of Argostoli is found to be  $S_{k,MV} \approx 150$  MVA and

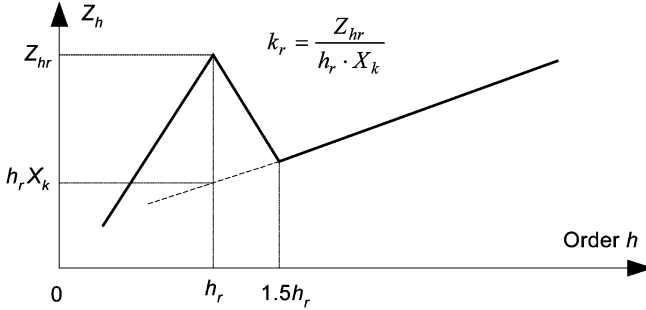


Fig. 15. System harmonic impedance approximation, using the “envelope impedance curve” [10].

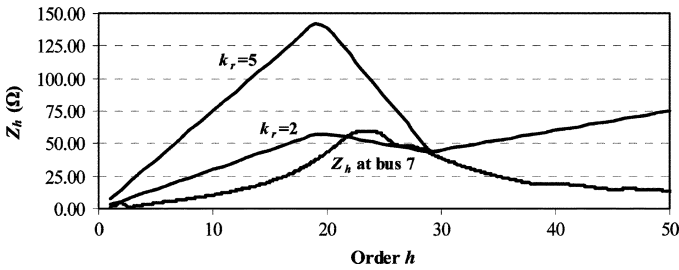


Fig. 16. “Envelope impedance curves” at the Argostoli MV bus and calculated system impedance (from Fig. 5, for minimum load).

$S_{k,HV} \approx 280$  MVA (varying with the system load and configuration). Hence, applying (7) with  $Q_c = 400$  kVar,  $f_r \approx 970$  Hz is obtained, or around the  $h_r = 19$ th harmonic order, which lies at the boundary of the high spectral content area in Fig. 4. Repeating this calculation for the HV side of the substation, using the total shunt capacitance of the HV cable and overhead lines ( $Q_c \approx 90$  MVar), a first resonance frequency around 90 Hz is found. Compared with the peaks in Figs. 5 and 6, the approximate calculation in both cases underestimates the resonance frequency by no more than 10%–15%.

For the given  $f_r$ , a conservative estimation of  $Z_h$  is provided by the “envelope impedance curve” of Fig. 15. The resonance amplification factor  $k_r$  depends on the damping effect of the load and according to [10], it varies between 2 and 5 in public distribution networks ( $k_r = 2$ –3 in [15], which is more realistic). The  $Z_h$  curve calculated with this method for the Argostoli MV bus is shown in Fig. 16 (for  $k_r = 2$  and  $k_r = 5$ ). Compared with the  $Z_h$  curve of Fig. 5 (included also in Fig. 16), the approximate curves are very conservative, even for the lowest values of  $k_r$ .

Proceeding one step further with the simplified IEC methodology, the harmonic current injections are needed for the whole wind farm, obtained from the current harmonics of a single WT (Fig. 4), applying (2). The WT and wind farm harmonics are both shown in Fig. 17, to demonstrate the attenuation of higher order harmonics by using increased values for the summation exponent  $a$  in (2).

Using the  $k_r = 2$  impedance curve of Fig. 16 and the wind farm current injections of Fig. 17, the voltage harmonics at the PCC are calculated using (6) and shown in Fig. 18. In the diagram, the harmonic load-flow results using the simplified MV network model are also shown. The simplified method, while

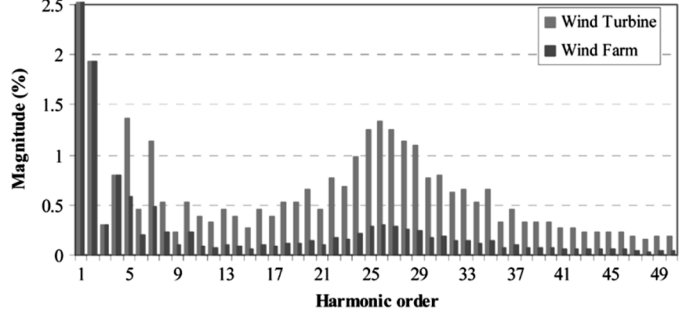


Fig. 17. Wind turbine and wind farm current harmonics (in percentage of respective rated values), applying the summation rule of (2).

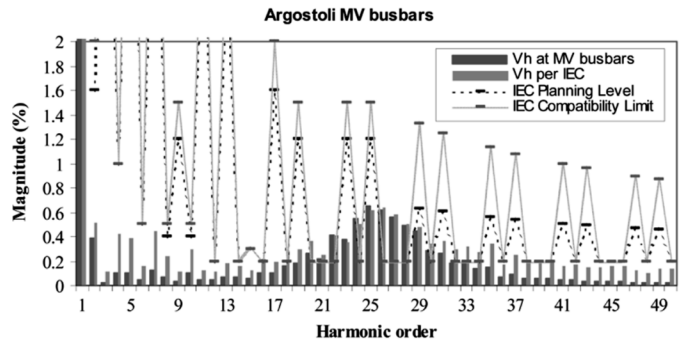


Fig. 18. Calculated voltage harmonics at the Argostoli MV busbars using the simplified method and from the harmonic load flow (Fig. 12).

overestimating the distortion outside the resonance region, is rather acceptable in the range of interest (admittedly with the assisted selection of the appropriate value for  $k_r$ ). Compared with the more accurate results of Fig. 13, the IEC method would be quite pessimistic. Yet, taking into account the simplifications and uncertainties already present in the harmonic analysis of Section IV, it appears that the simplified IEC method indeed provides a “rule-of-thumb” for a fast and conservative harmonic assessment.

## APPENDIX B

Since the output current harmonics of a WT stochastically vary with time, probabilistic techniques need to be applied for evaluating the total harmonic current of a wind farm and even more so the resulting harmonic distortion of the system voltages [16], [17]. This is also aligned with the statistical approach adopted in the IEC 61 000 series of electromagnetic-compatibility (EMC) standards, where harmonic emission coordination mainly refers to 95% nonexceeding probability values. Although an extensive treatment of this subject is beyond the scope of the paper, a discussion on the summation of harmonics in a wind farm is included in the Appendix, focusing on the high-order (switching frequency) harmonics, mainly to shed some light on the underlying assumptions in the application of (2).

Considerations and techniques for the summation of random vectors are presented in [16]–[18] and in several references provided therein. The manipulation of analytical relations in the probabilistic analysis of similar problems is laborious, and closed-form solutions are not always obtainable. For this reason, Monte Carlo simulation is often employed.

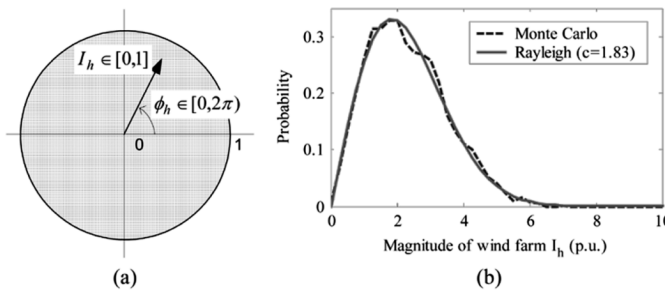


Fig. 19. Case A: (a) Root locus of individual WT harmonic current vectors for uniform magnitude and phase-angle distributions in  $[0, 1]$  and  $[0, 2\pi]$ . (b) The pdf of the wind farm harmonic current magnitude.

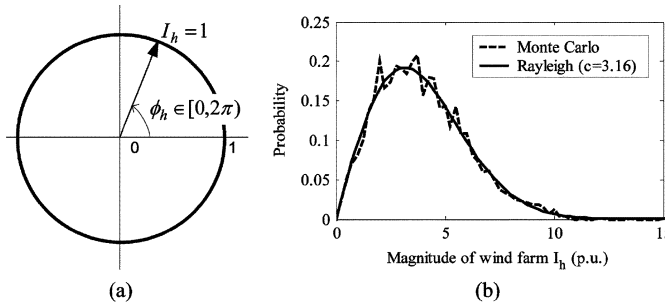


Fig. 20. Case B: (a) Root locus of individual WT harmonic current vectors for constant magnitude and uniform phase-angle distribution in  $[0, 2\pi]$ . (b) The pdf of the wind farm harmonic current magnitude.

The total harmonic current emissions of a wind farm will depend on the statistical characteristics of the individual WT harmonic current vectors [i.e., the probability distribution functions (pdf) of their magnitudes and phase angles (or of their real and imaginary components, if Cartesian coordinates are used)]. Joint probability distributions are utilized when statistical independence is not established.

When dealing with PWM-controlled converters, particularly with hysteretic current controllers as in this paper, it is reasonable to assume that the switching frequency harmonics of individual WTs are statistically independent random variables. Since the output current harmonics are not synchronized to the fundamental voltage waveform at the high frequencies of interest, their phase angles can be considered as uniformly distributed over the interval  $[0, 2\pi]$ .

The magnitudes of the individual harmonic vectors will also vary stochastically, depending on the prevailing wind conditions and the converter characteristics. PQ certificates of WTs provide the maximum magnitudes per harmonic order (10-min average values as per IEC 61 400-21), but no information on their distribution. To simplify the analysis, two characteristic situations are first examined.

**Case A)** The magnitudes of the individual WT harmonics are uncorrelated and uniformly distributed over the interval  $[0, 1]$  p.u. (1.0 p.u. is the maximum WT harmonic current).  
**Case B)** All magnitudes are equal to the maximum harmonic current (1.0 p.u.).

The respective loci of the WT harmonic current vectors for Cases A and B are, respectively, shown in Figs. 19(a) and 20(a).

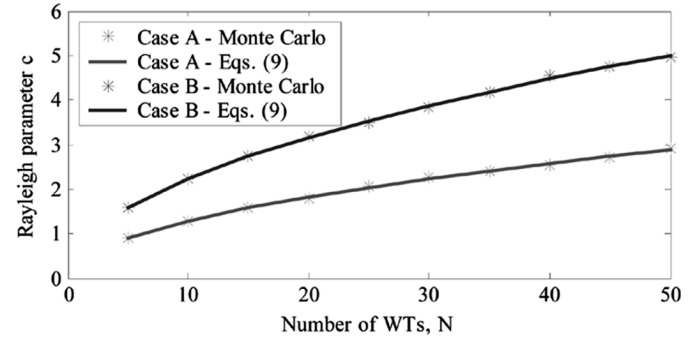


Fig. 21. Parameter  $c$  of the Rayleigh pdf of the wind farm harmonic current magnitude, calculated from the Monte Carlo simulation results and from the empirical (9), for Cases A and B.

TABLE II  
CHARACTERISTIC VALUES OF THE WIND FARM TOTAL HARMONIC CURRENT

	Mean, $\bar{I}$	Variance, $\sigma_I^2$	p-percentile, $I_p$
Case A	$\sqrt{\pi N/12}$	$(4 - \pi)N/12$	$\sqrt{-(N/3)\ln(1-p)}$
Case B	$\sqrt{\pi N/4}$	$(4 - \pi)N/4$	$\sqrt{-N\ln(1-p)}$

The magnitude of the total harmonic current of the wind farm for these simple cases follows a Rayleigh distribution (e.g., [16] and [18])

$$f(i) = \frac{i}{c^2} \exp\left(-\frac{i^2}{2c^2}\right) \quad (8)$$

where  $c$  is the distribution parameter. This is fully confirmed by Monte Carlo simulation in Figs. 19(b) and 20(b), for a wind farm consisting of  $N = 20$  WTs, as in the system of Fig. 3.

The relation between the parameter  $c$  of the Rayleigh distribution ( $c_A$  and  $c_B$ , for Cases A and B) and the number  $N$  of WTs is described by the following empirical equations:

$$c_A \cong \sqrt{\frac{N}{6}} \quad \text{and} \quad c_B \cong \sqrt{\frac{N}{2}} \quad (9)$$

derived from the results of repeated Monte Carlo simulations for a range of  $N$  values, plotted in Fig. 21. Using (9) for parameter  $c$  of the Rayleigh distribution, the mean, the variance, and the value of wind farm total harmonic current for a given nonexceeding probability  $p$  ( $p$ -percentile) can then be easily calculated. The results are tabulated in Table II.

To derive a single value for the wind farm harmonic current, a certain nonexceeding probability  $p$  needs to be adopted. Selecting a 95% probability, a level commonly used in the IEC 61 000 series of standards, and observing that  $\ln(1 - 0.95) = -2.9957 \cong -3$ , the wind farm harmonic current magnitudes obtained for Cases A and B are the following (in p.u. of the maximum harmonic current of a single WT)

$$I_{WF,95\%}^A \cong \sqrt{N} \quad \text{and} \quad I_{WF,95\%}^B \cong \sqrt{3N}. \quad (10)$$

Therefore, Case A leads to the standard summation rule of (2), whereas the 95% percentile current for Case B is  $\sqrt{3}$  times larger.

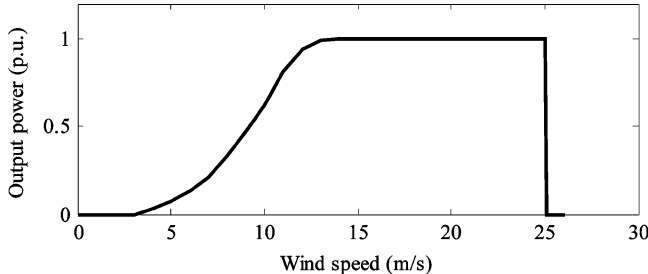
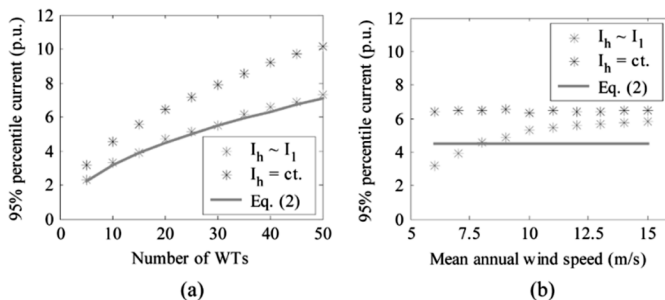


Fig. 22. WT power curve used for the simulations of Fig. 23.

Fig. 23. The 95% percentile magnitudes of the wind farm harmonic current for Case C as a function of (a) the number of WTs ( $V_w = 8$  m/s) and (b) the mean annual wind speed at a hub height (for  $N = 20$  WTs).

The assumption adopted in Case A, that the magnitudes of the individual WT harmonics are uncorrelated and vary uniformly from zero to the maximum value, is obviously questionable within the same wind farm, since the WTs will operate under similar (but not identical) conditions. On the other hand, the safe-side assumption made in Case B, that all turbines continuously operate at maximum distortion, may also be unrealistic.

Now, a more realistic study case is set up, which will be referred to as Case C. The magnitude of the current harmonics generated by each WT may, in general, depend on the operating point, as dictated by the prevailing wind speed at the wind farm installation area. Assuming a Rayleigh distribution for the 10-min average wind speed and using the WT power curve of Fig. 22, Monte Carlo simulation results for the 95% percentile of the wind farm total harmonic current are shown in Fig. 23, as a function of the number of WTs and the mean annual wind speed (at hub height). The WT availability factor has been also taken into account, with a value of 97%. In each diagram, two sets of points are shown. For the lower one, the WT current harmonics are assumed to vary in proportion to the output power of the WT. For the upper set, the current harmonics are assumed to be independent of the operating point, as may be the case for hysteresis controllers with a fixed hysteresis band. Variations due to wind field irregularities and other factors affecting the generated harmonics are also accounted for by assuming a uniformly distributed random variation of the harmonic current of each WT over an interval of 0.3-p.u. width.

In Fig. 23, the results obtained with the summation rule of (2) are also included. It is observed that (2) tends, in general, to underestimate the total harmonic current of the wind farm, particularly when the harmonic current spectrum does not vary considerably with the fundamental current (i.e., the output power) of the WTs. In this case, the calculated magnitudes exceed those obtained from (2) by a percentage of 44% (i.e.,  $\sqrt{2}$  times), which

remains practically constant, regardless of the prevailing wind conditions and number of WTs. Therefore, a more conservative (and rather “worse case”) summation rule, which might be used at high frequencies in place of (2), is the following:

$$I_h = \sqrt{2 \cdot \sum_k I_{h,k}^2}. \quad (11)$$

Nevertheless, it should be stressed that beyond any theoretical considerations, the technical evaluation procedure for a wind farm is always based on the application of relevant standards and guidelines. Presently, the relevant IEC documents covering this issue are [10] and [11], which stipulate the application of (2) for summing individual harmonic contributions from the WTs. For this reason, this summation rule has been applied to the harmonic load flows presented in this paper. Possibly, in future revised editions of these standards (particularly, [11]), the issue of harmonics summation will need further consideration, using measurements in actual installations, which the authors did not have the opportunity to conduct.

## REFERENCES

- [1] S. Heir, *Grid Integration of Wind Energy Conversion Systems*. New York: Wiley, 1998.
- [2] Harmonics, Characteristic Parameters, Methods of Study, Estimates of Existing Values in the Network 1981, CIGRE WG 36-05.
- [3] Guide for Assessing the Network Harmonic Impedance 1996, CIGRE WG CC02.
- [4] AC System Modeling for ac Filter Design—An Overview of Impedance Modeling 1996, CIGRE JTF 36.05.02/14.03.03.
- [5] “Modeling and simulation of the propagation of harmonics in electric power networks—Part I: Concepts, models and simulation techniques,” *IEEE Trans. Power Del.*, vol. 11, no. 1, pp. 452–465, Jan. 1996.
- [6] “Modeling and simulation of the propagation of harmonics in electric power networks—Part II: Sample systems and examples,” *IEEE Trans. Power Del.*, vol. 11, no. 1, pp. 466–474, Jan. 1996.
- [7] J. Arrillaga, B. C. Smith, N. R. Watson, and A. R. Wood, *Power System Harmonic Analysis*. New York: Wiley, 1998.
- [8] J. Arrillaga, N. R. Watson, and S. Chen, *Power System Quality Assessment*. New York: Wiley, 2000.
- [9] S. A. Papathanassiou, “A technical evaluation framework for the connection of DG to the distribution network,” *Elect. Power Syst. Res.*, vol. 77, no. 1, pp. 24–34, Jan. 2007.
- [10] Electromagnetic Compatibility (EMC) Part 3: Limits—Section 6: Assessment of Emission Limits for Distorting Loads in MV and HV Power Systems—Basic EMC Publication 1996, IEC 61 000-3-6.
- [11] Wind Turbine Generator Systems—Measurement and Assessment of Power Quality Characteristics of Grid Connected Wind Turbines 2001, IEC 61 400-21.
- [12] J. J. Grainger and W. D. Stevenson, *Power System Analysis*. New York: McGraw-Hill, 1994.
- [13] Z. Papazacharopoulos, K. Tatis, A. Kladas, and S. Manias, “Dynamic model for harmonic induction motor analysis determined by finite elements,” *IEEE Trans. Energy Convers.*, vol. 19, no. 1, pp. 102–108, Mar. 2004.
- [14] F. Santjer and R. Klosse, “Influence of transformers on harmonics,” presented at the Proc. Eur. Wind Energy Conf. (EWEC), Madrid, Spain, 2003, presented at the, unpublished.
- [15] C. Collombet, J. M. Lupin, and J. Schonek, *Harmonic Disturbances in Networks and Their Treatment*. : Schneider Electric, 1999, Cahier Technique no. 152.
- [16] Y. Baghizouz, “Time-varying harmonics: Part II—Harmonic summation and propagation,” *IEEE Trans. Power Del.*, vol. 17, no. 1, pp. 279–285, Jan. 2002.
- [17] A. Russo and P. Varilone, “Discussion of ‘Time-varying harmonics: Part II—Harmonic summation and propagation’,” *IEEE Trans. Power Del.*, vol. 18, no. 2, pp. 656–657, Apr. 2003.
- [18] A. Cavallini, R. Langella, A. Testa, and F. Ruggiero, “Gaussian modeling of harmonic vectors in power systems,” in *Proc. IEEE 8th Int. Conf. Harmonics and Quality of Power*, Athens, Greece, 1998, pp. 1010–1017.



**Stavros A. Papathanassiou** (S'93–M'98) received the Diploma in electrical engineering in 1991 and the Ph.D. degree in wind energy from the National Technical University of Athens (NTUA), Athens, Greece, in 1997.

He was with the Distribution Division of the Public Power Corporation of Greece, Athens, engaged in power quality and distributed generation studies, and was responsible for the elaboration of DG interconnection guidelines. In 2002, he became a Lecturer with the Electric Power Division of NTUA.

His research mainly deals with wind turbine technology and the integration of distributed generation in distribution networks.

Dr. Papathanassiou is a member of CIGRE, a registered professional engineer, and member of the Technical Chamber of Greece.



**Michael P. Papadopoulos** (M'88) received the Diploma in electrical and mechanical engineering and Ph.D. degrees from the National Technical University of Athens (NTUA), Athens, Greece, in 1956 and 1974, respectively.

In 1956, he joined the Public Power Corporation of Greece, where he was engaged in the planning, design, operation, and control of rural and urban distribution networks, as well as in the utilization of electric energy. In 1985, he joined the School of Electrical and Computer Engineering of NTUA, where he is a Professor in the Electric Power Division. From 2000 to 2004, he was a member of the Board of the Regulatory Authority for Energy of Greece. His research interests are in distribution systems and renewable energy sources.

Dr. Papadopoulos is a member of CIGRE, a registered professional engineer, and member of the Technical Chamber of Greece.